Tube Mechanism With 3-Axis Rotary Joints Structure to Achieve Variable Stiffness Using Positive Pressure

Issei Onda, Masahiro Watanabe, *Member, IEEE*, Kenjiro Tadakuma, Kazuki Abe, *Member, IEEE*, and Satoshi Tadokoro, *Fellow, IEEE*

***Abstract*—Studies on soft robotics have explored mechanisms for switching the stiffness of a robot structure. The hybrid soft-rigid approach, which combines soft materials and high-rigidity structures, is commonly used to achieve variable stiffness mechanisms. In particular, the positive-pressurization method has attracted significant attention in recent years as it can eliminate the constraints on driving pressure. Moreover, it can change the shape holding force according to internal pressure. In this study, a variable stiffness mechanism, comprising 3-axis rotary ball joints and a single chamber, was devised via frictional force using positive pressure. The prototype can change joint angles arbitrarily when no pressure is applied and can hold joint angles when positive pressure is applied. Using a theoretical model of the torque required to hold the joint angle, we simulated the holding torque using finite element modeling analysis and measured the holding torque in the pitch and roll directions when internal pressure was applied. Based on the interaction of the theoretical model, measurement, and FEM analysis, it was confirmed that the value of the holding torque in the roll direction was approximately $\pi/2$ times larger than that in the pitch direction for each value of the internal pressure. Further, we evaluated the FEM value, theoretical value, and measured value of the holding torque by performing pairwise numerical comparisons. Our approach will aid the design of effective stiffening mechanisms for soft robotics applications.**

***Index Terms*—Mechanism, positive-pressure driven, tubular structure, variable stiffness.**

I. Introduction

RECENT studies on soft robotics have explored mechanisms that can switch the stiffness of a robot structure. A flexible structure is necessary for robots to perform large passive and active deformations. In contrast, a highly rigid state is required for achieving precise position control to ensure that the external forces or weight of the robot do not deform. These mechanisms are expected to have various applications in which both functions are required and can be achieved by switching the stiffness.

The hybrid soft-rigid approach [1], [2], which combines soft materials and high-rigidity structures, is commonly used for variable-stiffness mechanisms. A few instances of such meth-ods include bulk and longitudinal locking using negative pressure [3], [4], [5], [6], [7], [8], segment locking using a wire [9], [10], [11], [12], and phase transition using temperature [13], [14], [15], [16], [17], [18].

The bulk and longitudinal locking methods, which can switch the stiffness using friction, apply a negative pressure to the particles [3], [4], [5] or layers [6], [7], [8] inside a bag such that they come in contact with each other and increase the stiffness. This method arbitrarily determines the shape of the bag used to cover the filling. The bag can significantly deform under an external force in the absence of negative pressure. However, the maximum driving pressure is 0.1 MPa. Additionally, because the contents must be covered with a flexible membrane, the membrane may be damaged and malfunction when contacted by sharp objects.

The segment locking method using a wire [9], [10], [11], [12] can increase the stiffness by applying tension to the wire. The wire passes through an articulated structure consisting of multiple segments. The frictional force generated by pulling the wire stiffens the structure. However, the friction between the wire and the inner surface of the wire guide may result in a significant loss in the shape-holding force.

The temperature-based phase transition methods include the low-melting-point alloy method [13], [14], [15] and the low-melting-point polymer method [16], [17], [18]. Under the liquid phase, the alloy deforms easily, and under the solid phase, there is a considerable difference in stiffness compared to the liquid phase. The responsiveness during the shift in the stiffness is low because the phase transition is time consuming.

In addition to these aforementioned methods, the positive-pressurization method has attracted attention in recent years owing to its unique features, such as the absence of a limit on the driving pressure. The low responsiveness of the switching stiffness under large structure volumes can be mitigated by increasing pressure. Moreover, the positive-pressurization method can continuously change the shape-holding force according to internal pressure.

Previous research has been conducted on positive-pressurization methods, such as rescue manipulator [19], tubular jammed beam [20], pressure-driven manipulator [21], and tool holding articulated arm [22]. Rescue manipulator [19] uses a semicircular duplex mechanism to propel itself in an arbitrary

Manuscript received 30 September 2022; accepted 23 December 2022. Date of publication 6 January 2023; date of current version 4 December 2023. This letter was recommended for publication by Associate Editor G. Endo and Editor C. Gosselin upon evaluation of the reviewers' comments. This work was supported in part by MEXT Grant-in-Aid for Scientific Re-search on Innovative Areas, Science of Soft Robot Interdisciplinary Integration of Mechatronics, Material Science, and Bio-Computing under Grant 18H05471 and in part by JST [Moonshot R&D – MILLENIA Program] under Grant JPMJMS2034. *(Corresponding author: Kenjiro Tadakuma.)*

Issei Onda and Satoshi Tadokoro are with the Graduate School of Information Sciences, Tohoku University, Sendai, Miyagi 980-8577, Japan (e-mail: onda.issei@rm.is.tohoku.ac.jp; tadokoro@rm.is.tohoku.ac.jp).

Masahiro Watanabe, Kenjiro Tadakuma, and Kazuki Abe are with the Tough Cyberphysical AI Research Center, Tohoku University, Sendai, Miyagi 980-8577, Japan (e-mail: watanabe.masahiro@rm.is.tohoku.ac.jp; tadakuma@rm.is.tohoku.ac.jp; kazuki.abe.org@gmail.com).

This letter has supplementary downloadable material available at https://doi.org/10.1109/LRA.2023.3234767, provided by the authors.

Digital Object Identifier 10.1109/LRA.2023.3234767

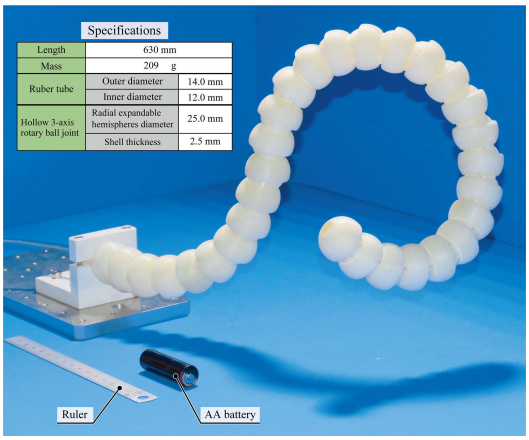

Fig. 1. Prototype of the proposed mechanism and prototype specifications.

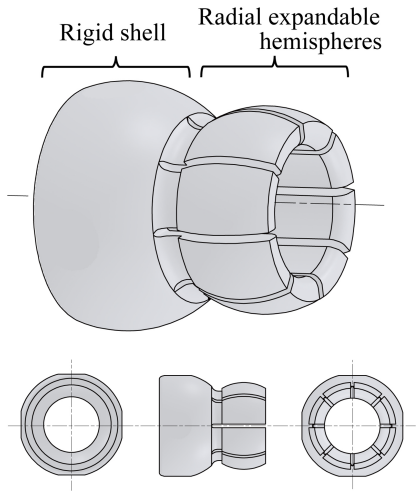

Fig. 2. 3-axis rotary ball joint design of the proposed method.

direction. However, the robot consists of numerous parts and has a complex structure. Tubular jammed beams [20] and multiple tubes have been placed inside a thin-walled pipe and expanded to increase the stiffness through contact between the tubes. The principles and structures are simple; however, when the tube is expanded, its shape becomes straightened. Pressure-driven manipulator [21] comprises a link structure that connects single-axis rotary joints, and the structure becomes highly rigid owing to the friction between the rubber chamber and rigid walls. However, this mechanism includes only one degree of freedom for the joints and uses multiple chambers. Tool holding articulated arm [22] becomes highly rigid by contacting the ball joint, presser, and housing pushed by the spring when no pressure is applied. When pressure is applied, the arm becomes flexible as it does not contact these parts. However, this arm has a complicated structure and sliding resistance because it contains an air cylinder.

In this study, we devised a variable stiffness mechanism via frictional force using positive pressure with a 3-axis rotary joint and a single chamber. The proposed mechanism has an articulated structure based on a linked 3-axis rotary joint that can deform freely when internal pressure is not applied and achieves high stiffness when internal pressure is applied. The specific mechanism consists of a cylindrical rubber tube enclosed inside a ball-joint-type segment [23] (Fig. 1 and Supplementary Movie) and a McKibben pneumatic artificial muscle enclosed inside a bead-type segment [24]. These methods facilitate variable stiffness functions by extending and contracting the force in an enclosed chamber. For the joint shape in our proposed method, although it is necessary to provide an expandable hemisphere (Fig. 2) in the ball joint type, only a hollow male-female joint structure is required. Although the number of joints increases with the total length of the structure, the only components required to form an articulated structure were the joints, chambers, and fittings to keep the chambers sealed. In addition, the proposed mechanism does not have any sliding resistance.

Although the concept of the positive-pressure variable stiffness mechanism has been demonstrated, a design method for the ball joint type has not yet been established. The theoretical and experimental values of the performance, assemblability, and limitations of critical parameters, such as the joint holding torque, whether the expandable hemisphere fits into the shell, and whether the expandable hemisphere dislocates from the shell during pressurization, are unclear. Therefore, the purpose of this study is to construct a design method based on the interaction of a theoretical model, finite element modeling with nonlinear analysis, and actual measurements.

The remainder of this letter is organized as follows. Section II presents the basic principle of the mechanism and the theoretical model for fitting the shell, whether to dislocate the shell, and the holding torque. Section III discusses the design of the joint design and explains the prototype configuration. Section IV discusses the analytical and experimental results obtained using theoretical equations, FEM simulations, and measurements of the holding torque. Section V discusses the limitations of this study. Section VI summarizes the study and discusses future research.

II. Basic Principle

A. Positive-Pressure Driven Variable Stiffness Mechanism

The design of positive-pressurization method is different from that of the negative-pressurization method, in which variable stiffness is achieved through friction. This is because the geometry of the structure must be designed such that it caters to the direction of the force exerted by the positive-pressure method. In the negative-pressurization method, even if the elements are enclosed inside the chamber, they can withstand external pressure and can be held in any shape. In contrast, a positive-pressurization method with the same configuration as the negative-pressurization method cannot withstand internal pressure, and it would be difficult to hold it in an arbitrary shape.

In this letter, we propose an articulated shape-holding mechanism using a positive-pressure method that can retain geometric constraints in the axial and radial directions, independent of the joint angle. This method requires placing firm shells outside the chamber to constrain the tensile force generated in the expanding chamber.

The 3-axis rotary ball joint of the proposed mechanism is shown in Fig. 2. The ball joints have a hemispherical rigid shell and a radial expandable hemisphere with slits in the longitudinal direction. This shape simplifies the structure when the ball joint is assembled. The shell cannot be deformed, thereby preventing the rubber tube from being damaged by sharp external objects. Fig. 3 shows the working principle of the proposed mechanism. This mechanism has a linked structure with 3-axis rotary ball

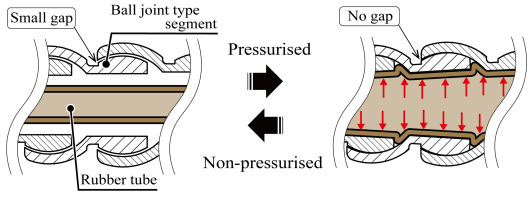

Fig. 3. Principle of the proposed method for variable stiffness.

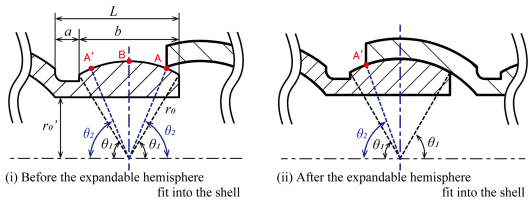

Fig. 4. Fitting of expandable hemisphere on shell.

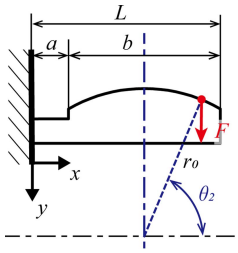

Fig. 5. Stepped cantilever under concentrated load.

joints and an enclosed rubber tube that passes through the structure. The expandable hemisphere is deformed by pressurizing the enclosed rubber tube, and contact pressure is obtained between the expandable hemisphere and shell.

B. Theoretical Model of the Expandable Hemisphere That Can Be Fitted to the Shell

Here, we explain the model of the expandable hemisphere and shell. Fig. 4(i) shows a cross-sectional view of the expandable hemisphere before fitting it into the shell. Here, L is the total length of the expandable hemisphere, a is the length of the base of the expandable hemisphere, b is the length of the contact area between the expandable hemisphere and the shell, r_0 is the outer radius of the expandable hemisphere at $a \leq x \leq L$, r_0' is the inner radius of the expandable hemisphere; θ_2 ($0 \leq \theta_2 \leq \pi/2$) is the angle to contact point A, and θ_1 is the range from the central axis to the tip of the expandable hemisphere.

When the shell is fitted onto the expandable hemisphere, we assume that the shell is a rigid body and that the shell and expandable hemisphere come into contact at point A, as shown in Fig. 4. As the shell slides further, the expandable hemisphere is deformed, and the edge of the shell reaches point A'. Because the cross-sectional shape of the contact area between the expandable hemisphere and the shell is axisymmetric, the angle to point A' is θ_2, as shown in Fig. 4(ii).

We consider a stepped cantilever deflected by a concentrated load F applied to point A (Fig. 5). For the expandable hemisphere to fit into the shell, the deflection δ at $x = a + b/2$ must be larger than $r_0(1-\sin\theta_2)$. The distance to point A is $a + (b/2) + r_0\cos\theta_2 = t$, moment of inertia of area $0 \leq x \leq a$ is I_1, and moment of inertia of area $a \leq x \leq L$ is I_2.

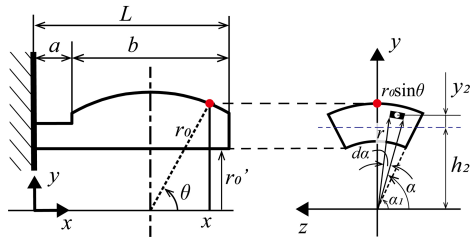

Fig. 6. Moment of inertia of area I_2.

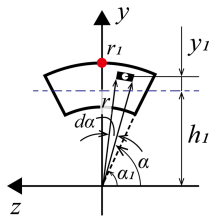

Fig. 7. Moment of inertia of area I_1.

Because the moment of inertia of area I_2 is non-uniform, we must consider it as a function of x. To obtain I_2, we consider the cross-section of the stepped cantilever at an arbitrary point $x = a + (b/2) + r_0\cos\theta$, as shown in Fig. 6. The range of θ is $\theta_1 \leq \theta \leq \pi/2$. Here, r is the radius to the differential area, α is the angle to the differential area on the y–z plane, α_1 is the angle to the edge of the cantilever on the y–z plane, h_2 is the distance to the neutral axis, and y_2 is the distance from the neutral axis to the differential area, and can be represented as follows.

$$y_2 = r\sin\alpha - h_2 \tag{1}$$

To obtain the moment of inertia of area I_2 at an arbitrary point, θ is converted to x as follows.

$$\theta = \cos^{-1}\left(\frac{x - a - \frac{b}{2}}{r_0}\right) \tag{2}$$

Next, the moment of inertia of the area I_{z2} about the z-axis is calculated as follows:

$$I_{z2} = 2\int_{\alpha_1}^{\frac{\pi}{2}}\int_{r_0'}^{r_0\sin\theta}(r\sin\alpha)^2 \cdot r \cdot d\alpha \cdot dr \tag{3}$$

Additionally, the cross-sectional area A_2 at $a \leq x \leq L$ is as follows.

$$A_2 = \pi\left(r_0^2\sin^2\theta - r_0'^2\right)\frac{\pi - 2\alpha_1}{2\pi} \tag{4}$$

The distance h_2 to the neutral axis is obtained as follows.

$$2\int_{\alpha_1}^{\frac{\pi}{2}}\int_{r_0'}^{r_0\sin\theta}(r\sin\alpha - h_2) \cdot r \cdot d\alpha \cdot dr = 0 \tag{5}$$

From these equations, the moment of inertia of area I_2 about the neutral axis is expressed by the parallel-axis theorem, as follows:

$$I_2 = I_{z2} - h_2^2 A_2 \tag{6}$$

Similarly, the moment of inertia of area $0 \leq x \leq a$ is I_1 shown in Fig. 7 is as follows.

$$y_1 = r\sin\alpha - h_1 \tag{7}$$

$$I_{z1} = 2\int_{\alpha_1}^{\frac{\pi}{2}}\int_{r_0'}^{r_1}(r\sin\alpha)^2\cdot r\cdot d\alpha\cdot dr \tag{8}$$

$$A_1 = \pi\left(r_1^2 - r_0'^2\right)\frac{\pi - 2\alpha_1}{2\pi} \tag{9}$$

$$2\int_{\alpha_1}^{\frac{\pi}{2}}\int_{r_0'}^{r_1}(r\sin\alpha - h_1)\cdot r\cdot d\alpha\cdot dr = 0 \tag{10}$$

$$I_1 = I_{z1} - h_1^2 A_1 \tag{11}$$

where y_1 is the distance from the neutral axis to the differential area, r_1 is the outer radius of the expandable hemisphere at $0 \le x \le a$, I_{z1} is the moment of inertia of the area, A_1 is the cross-sectional area at $0 \le x \le a$, and h_1 is the distance to the neutral for $0 \le x \le a$ and $a \le x \le t$, respectively, are expressed below.

$$\frac{d^2y}{dx^2} = \frac{F}{EI_1}(t-x)\ (0 \le x \le a) \tag{12}$$

$$\frac{d^2y}{dx^2} = \frac{F}{EI_2}(t-x)\ (a \le x \le t) \tag{13}$$

where E is Young's modulus. Here, the 5th order Taylor expansion is calculated around $x = a$ to reduce the computational cost of the differential equation of deflection for $a \le x \le t$. $x = a$ is used as an expansion point because of the boundary of the stepped beam, and the deformation at this point must be accurately estimated. The accuracy of the approximate deformation of the beam near $x = L$ is not critical.

Additionally, the boundary condition is as follows.

$$y = 0\ (x = 0) \tag{14}$$

$$\frac{dy}{dx} = 0\,(x = 0) \tag{15}$$

$$\frac{dy}{dx}_{|x=a-0} = \frac{dy}{dx}_{|x=a+0} \tag{16}$$

$$y_{|x=a-0} = y_{|x=a+0} \tag{17}$$

From the boundary conditions, F can be calculated when the deflection is $\delta = r_0(1\text{-}\sin\theta_2)$ at $x = a + (b/2)$. Consequently, the bending stress σ owing to the maximum bending moment Mmax $(x = 0)$ at F is obtained. Bending stress σ is expressed as follows:

$$\sigma = \frac{M_{\max}}{I_1}(r_1 - h_1) = \frac{Ft}{I_1}(r_1 - h_1) \tag{18}$$

From (18), it can be inferred that the expandable hemisphere can fit into the shell without breaking if the maximum bending allowable stress σ' is not exceeded. Specifically, θ_2 $(0 \le \theta_2 \le \pi/2)$ should be greater than a specific threshold value for the shell to fit without breaking the expandable hemisphere.

C. Theoretical Model of Expandable Hemisphere That Does Not Dislocate From the Shell When Pressurized

Here, the mechanism of the expandable hemisphere dislocates from the shell is explained. When pressurized with the expandable hemisphere fitted in the shell, expansion forces are generated in the radial and axial directions of the rubber tube at the contact point A' in Fig. 8. If the expandable hemisphere has no stiffness, the following conditions must be fulfilled to prevent the shell from dislocating owing to the expansion force:

$$\mu\left(PS\sin\theta_2 + T\cos\theta_2\right) + PS\cos\theta_2 > T\sin\theta_2 \tag{19}$$

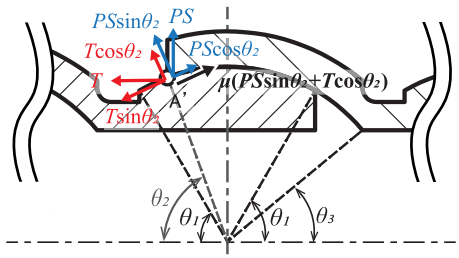

Fig. 8. Expansion force at the contact point A'.

$$\mu\left(PS\sin\theta_2 + PS'\cos\theta_2\right) + PS\cos\theta_2 > PS'\sin\theta_2 \tag{20}$$

where, μ is the static friction coefficient, P is the internal pressure, T is the expansion force in the axial direction, θ_2 is the range of the shell covering the expandable hemisphere, S is the pressure area in the radial direction, and S' is the pressure area in the axial direction. The pressure areas S and S' are expressed as follows:

$$S = 2\pi r_0' L \tag{21}$$

$$S' = r_2^2\pi + \int_{\theta_3}^{\theta_1} 2\pi r_0^2\sin\theta\cdot d\theta. \tag{22}$$

r_2 is the radius of air plug for gluing the end of the rubber tube and θ_3 is the angle to the end of the inner sphere of the shell. The force in the radial direction is determined by the pressure area of the radial expandable hemisphere, including the slits. The axial direction force is determined by the pressure area of the air plug and the inner sphere of the shell.

If the expansion in the radial and axial directions of the rubber tube and the deformation in the expandable hemisphere are minimized, it can be assumed that there is no internal pressure loss owing to these deformations.

From (20), if the frictional and radial tangential forces are larger than the tangential force in the axial direction, the expandable hemisphere will not dislocate.

However, because (20) does not consider the stiffness of the expandable hemisphere, it can be inferred that the limit values of the internal pressure and the range of the shell when the expandable hemisphere does not dislocate are greater than the theoretical values. Therefore, in addition to the theoretical model, we use the FEM and prototype to discuss the prevention of expandable hemisphere dislocation from the shell considering the stiffness in Sections III-B and IV-A.

D. Theoretical Model of Holding Torque

We constructed a model to calculate the theoretical values of holding torque in the pitch and roll directions. The normal directional force on the differential area of the shell is calculated (Fig. 9). The distance from the center of rotation of the joint to the differential area is r_0. The angle around the z-axis is θ, while that around the x-axis is β.

The holding torques in the pitch and roll directions are τ_1 and τ_2, respectively; the distances to the rotation center of these torques are different. The distance r_{xy} to the differential area in Fig. 9(ii) and distance r_{yz} to the differential area on the circumference of radius $r_0\sin\theta$ in Fig. 9(ii) are as follows:

$$r_{xy} = r_0\ \sin\theta \tag{23}$$

$$r_{yz} = r_0\ \sin\theta\cos\beta \tag{24}$$

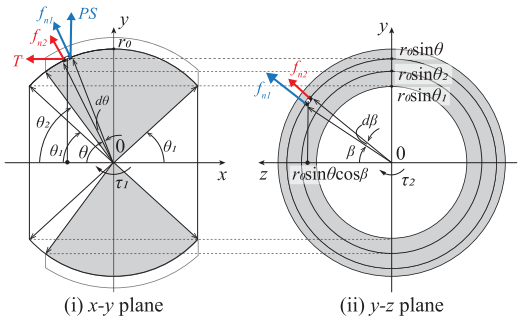

Fig. 9. Normal force on differential area of joint shell.

TABLE I
PARAMETERS FOR DESIGNING 3-AXIS ROTARY BALL JOINT

Total length of the expandable hemisphere	L [mm]	15.5
Length of the base of the expandable hemisphere	a [mm]	3.0
Length of the contact area	b [mm]	12.5
Outer radius of the expandable hemisphere	r_0 [mm]	12.5
Inner radius of the expandable hemisphere	r_0' [mm]	8.0
Range from the central axis to the tip of the expandable hemisphere	θ_1	$\pi/3$
Angle to the edge of the cantilever on the yz plane	α_1	$3\pi/8$
Outer radius of the expandable hemisphere at $0 \le x \le a$	r_1 [mm]	10.0
Young's modulus	E [MPa]	3530
Maximum bending allowable stress	σ' [MPa]	110
Coefficient of static friction	μ	0.1735
Radius of air plug for gluing the end of the rubber tube	r_2 [mm]	6.0
Angle to the end of the inner sphere of the shell	θ_3	0.694
Pressure area in the radial direction	S' [mm^2]	779.1
Pressure area in the axis direction	S' [mm^2]	376.6

(23) and (24) indicate the distance to the rotation center of the holding torque in the roll and pitch directions, respectively.

f_{n1} and f_{n2} are the normal forces obtained from the radial and axial forces in a differential area, respectively. At this time, the tangential force caused by the expansion of the rubber tube cancels out; thus, it does not affect the holding torque.

The expansion force in the radial direction of the rubber tube is assumed to be transmitted in the vertical upward direction. The expansion force of the rubber tube in the radial direction is transmitted to the shell on a spherical surface within the range of $\theta_2 \le \theta \le \pi - \theta_1$ and $0 \le \beta \le \pi/2$. The expansion force in the axial direction is transmitted to the shell within the range of $\theta_2 \le \theta \le \pi/2$ and $0 \le \beta \le \pi/2$.

f_{n1} and f_{n2} are obtained as follows.

$$f_{n1} = PS \sin\theta \tag{25}$$

$$f_{n2} = T cos\theta \ = \ PS' \cos\theta \tag{26}$$

From (25) and (26), the stresses σ_1 and σ_2, which are forces per unit area in the radial and axial directions, are as follows.

$$\sigma_1 = \frac{f_{n1}}{4\int_0^{\frac{\pi}{2}} \int_{\theta_2}^{\pi-\theta_1} r_0 d\theta \cdot r_0 \sin\theta d\beta} \tag{27}$$

$$\sigma_2 = \frac{f_{n2}}{4\int_0^{\frac{\pi}{2}} \int_{\theta_2}^{\frac{\pi}{2}} r_0 d\theta \cdot r_0 \sin\theta d\beta} \tag{28}$$

From (23) to (28), the holding torques τ_1 in the pitch direction and τ_2 in the roll direction are expressed by

$$\tau_1 = 4\int_0^{\frac{\pi}{2}} \int_{\theta_2}^{\pi-\theta_1} \mu\sigma_1 \cdot r_0 \sin\theta \cos\beta \cdot r_0 d\theta \cdot r_0 \sin\theta d\beta + 4\int_0^{\frac{\pi}{2}} \int_{\theta_2}^{\frac{\pi}{2}} \mu\sigma_2 \cdot r_0 \sin\theta \cos\beta \cdot r_0 d\theta \cdot r_0 \sin\theta d\beta \tag{29}$$

$$\tau_2 = 4\int_0^{\frac{\pi}{2}} \int_{\theta_2}^{\pi-\theta_1} \mu\sigma_1 \cdot r_0 \sin\theta \cdot r_0 d\theta \cdot r_0 \sin\theta d\beta + 4\int_0^{\frac{\pi}{2}} \int_{\theta_2}^{\frac{\pi}{2}} \mu\sigma_2 \cdot r_0 \sin\theta \cdot r_0 d\theta \cdot r_0 \sin\theta d\beta \tag{30}$$

In particular, (29) and (30) indicate that the holding torque in the roll direction is $\pi/2$ times larger than that in the pitch direction.

III. MECHANICAL DESIGN

A. Design Method of 3-Axis Rotary Ball Joint

In this section, based on the theoretical models presented in Sections II-B and II-C, we discuss the design of a joint that can be assembled, and that is not dislocated when a positive pressure is applied. In this letter, the joints were machined using MC nylon (MC901) because of its high dimensional stability, high mechanical strength, abrasion resistance, and high toughness.

First, based on the theoretical model discussed in Section II-B, we determined the shell range θ_2 for designing a joint that could be assembled. Table I lists all the parameters necessary to design the joint. The result of calculating the shell range θ_2 using the parameters shown in Table I and the numerical analysis software "MATLAB" is as follows.

$$\theta_2 = \ 64.22 \ [\text{deg}] \tag{31}$$

Here, θ_2 must be larger than the value in (31) to design a joint that can be assembled. Therefore, we set θ_2 to 65°, considering the reliability of the assembly and because the movable range of the joint and the maximum angle of θ_2 are $\pi/2$.

Additionally, we substituted the determined θ_2 into (20) in II.C and examined whether the expandable hemisphere dislocates from the shell at internal pressures of 0.1 MPa, 0.2 MPa, and 0.3 MPa. We confirmed that the left side of (20) was greater than its right side at all internal pressures. Therefore, the shell range θ_2 in this letter is 65°.

B. Design of the Prototype of the Proposed Mechanism

Fig. 10(a) shows the 3-axis rotary ball joint based on Section III-A and Table I. The shell thicknesses of the joints in this letter is 2.5 mm. Eight expandable hemispheres are required to unify the arrangement of the expandable hemispheres in both the pitch and yaw directions. The gap between the expandable hemispheres is 1 mm, which is the same thickness of the rubber tube used. Additionally, the gap between the expandable hemisphere and the shell is 0.1 mm.

The rubber tube (Fig. 10(b)) has outer and inner diameters of 14 mm and 12 mm, respectively, and a thickness of 1 mm. This is because the inner diameter of the expandable hemisphere is 16 mm, and the pressure loss owing to the expansion of the rubber tube is ignored. The rubber tube is made of Ecoflex 00-50, the same material and fabrication as the rubber tube used in [21].

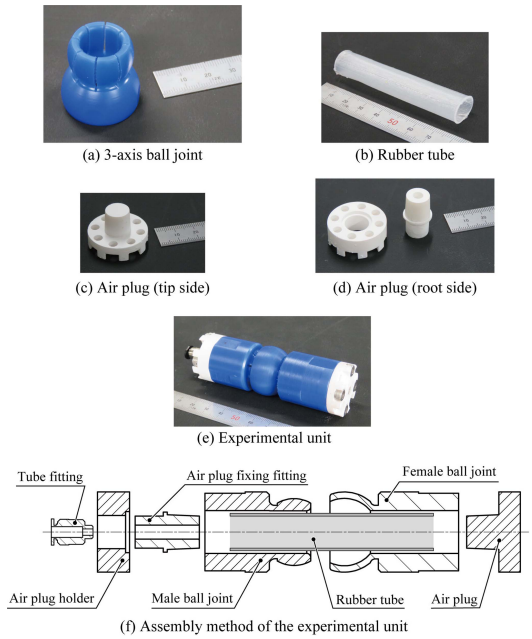

Fig. 10. Parts and assembly of prototype for the proposed method.

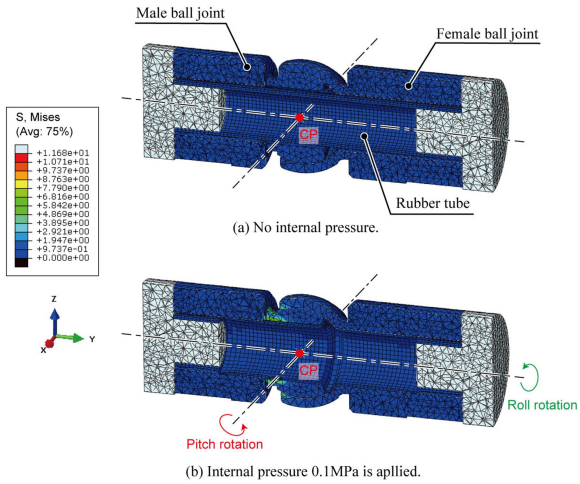

Fig. 11. 3D experimental setup in FEM simulations for evaluating the holding torque. To obtain holding torque in pitch direction, rotate female joint around the CP in the *x*-axis. To output holding torque in the roll direction, rotate female joint around the CP in y-axis.

The air plug (Fig. 10(c) and (d)) for gluing the ends of the rubber tube consists of a taper. The diameters of the tapered tip and tapered root are 12 mm and 13 mm, respectively, and the length of the tapered part is 12 mm. The plugs are made of resin-containing glass (Rigid 10 K) and manufactured using stereolithography (Formlabs, Form 3, USA). The plug on the root side is divided into two parts for ease of assembly.

The assembly method for the experimental unit is shown in Fig. 10(e) and (f). The tip and root air plugs are glued to a rubber tube. A rubber tube with an air plug is inserted into the female joint, and the air plug is connected to the female joint. The male joint fits into the female joint. Finally, the root air plug is inserted into the holder and the tube fitting is fixed to the root air plug. The expandable hemisphere of the male joint was not broken when the experimental setup was assembled. In addition, the expandable hemisphere of the male joint was not dislocated from the shell of female joint when 0.2 MPa is applied.

IV. Simulation and Experiment

A. Simulation of Holding Torque Using Finite Element Analysis

In this subsection, we performed a finite element analysis using Abaqus/CAE (Dassault Systems, France) to evaluate the holding torque obtained using the proposed mechanism, including the rubber tube. A 3D model was created using Abaqus to compare the theoretical model values with the actual measured values. The joint and rubber tubes were of the same scale as the model used in the experiment. However, the air plug used a model without a taper to constrain it using a rubber tube. The diameter of the constraining part of the air plug was 12 mm, which is the same as the inner diameter of the rubber tube.

We explain the definitions of the joints and rubber tubes in Abaqus. The material of the joint and air plug is MC nylon (MC901), and according to the datasheet, Young's modulus and Poisson's ratio are 3530 MPa and 0.4, respectively. The material of the rubber tube is Ecoflex 00-50, which is defined by the 3rd order of the Ogden hyper elastic model from the material parameters in [21].

The coefficient of static friction between MC nylon (MC901) is 0.1735, and the coefficient of static friction between MC nylon (MC901) and Ecoflex 00-50 is 1.431. These values are measured according to the ISO 15113:2005 (Rubber - Determination of frictional properties) standard (Procedure A).

We applied internal pressures of 0.1, 0.125, 0.15, 0.175, and 0.2 MPa to the inner wall of the rubber tube and the air plug constraining the rubber tube, and then obtained the joint holding torque from the radial and axial forces. After confirming the prevention of expandable hemisphere dislocation from the shell, the female joint was rotated at a maximum angle of 5° in the pitch and roll directions, and the maximum value of the moment around the central point (CP) for rotation was the output (Fig. 11 and Supplementary Movie). The FEM values are shown in Section IV-B along with the theoretical and measured values.

B. Measuring the Holding Torque in the Pitch and Roll Directions

In this subsection, we present the measurements of the holding torque in the pitch and roll directions for comparison with theoretical and FEM values. Figs. 12 and 13 show the devices used to measure the holding torque in the pitch and roll directions, respectively (Supplementary Movie).

We measured the tensional force in the pitch and roll directions when the wire connector was rotated to measure the maximum static friction force when using an experimental setup. In this experiment, the wire connector was pulled by a wire with a spring that was tied to a tensile testing machine (Model 3343, INSTRON, Japan) when internal pressure was applied. The pulling force at each internal pressure was measured five times, and the average values of the friction force were obtained accordingly. The holding torque was calculated by multiplying the obtained maximum static friction force value and the length from the center of rotation to the tip of the wire connector. The wires used in the experiments were made of stainless steel. A high-precision regulator (IR1020-01, ISE30A-01, SMC, Japan) was used to control the internal pressure.

Experimental conditions:

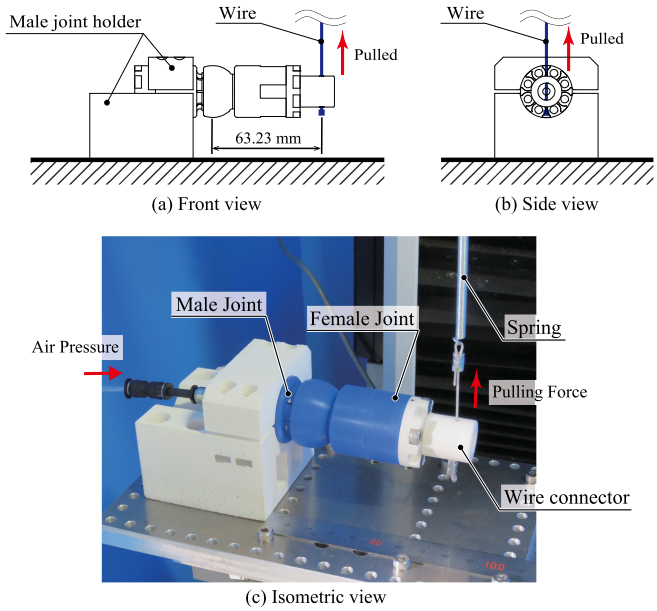

Fig. 12. Experimental setup for measuring the holding torque in the pitch direction. This setup offset the moments due to the weight of the arm from the measured value. Holder and connector are made of resin containing glass (rigid 10K) and are manufactured using stereolithography (formlabs, form 3, USA).

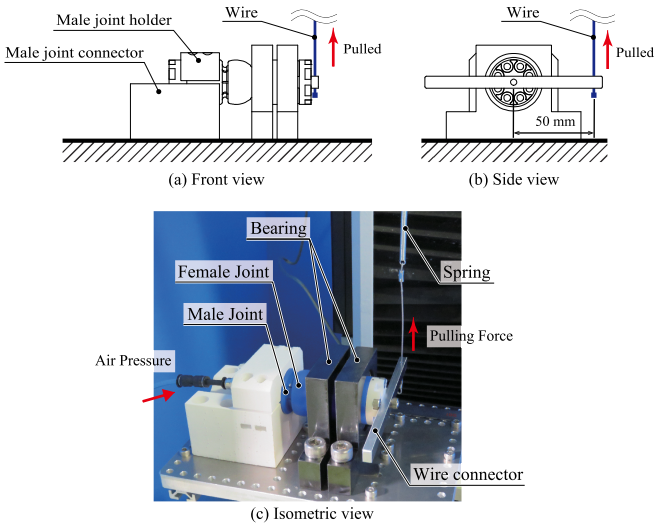

Fig. 13. Experimental setup for measuring the holding torque in the roll direction. Wire connector is made of machined duralumin (A2017).

- The applied pressures were 0.1, 0.125, 0.15, 0.175, and 0.2 MPa.
- The moment arm lengths were 63.23 mm in the pitch direction and 50 mm in the roll direction, as shown in Figs. 12 and 13, respectively.
- The pulling velocity was 30 mm/min.
- The product number of the spring used was 3.96 × 79.3 of the 200PC SPRING ASSORTMENT. The spring constant was determined to be 0.783.
- The maximum pulling extension was 10 mm to measure the maximum static friction force in the pitch and roll directions.

Fig. 14 shows the theoretical, FEM, and measured values of the holding torque in the pitch and roll directions for each

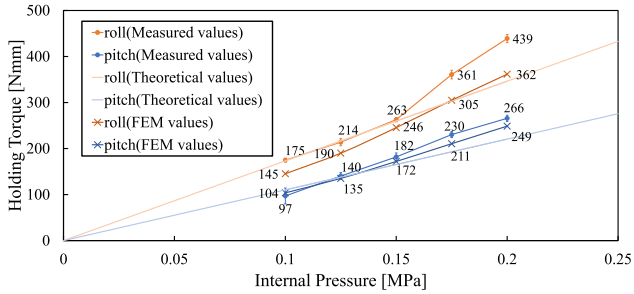

Fig. 14. Results of theoretical, FEM, and measured values of holding torque in pitch and roll directions. The error bar indicates the standard deviation of the measured value.

TABLE II
MAGNIFICATION OF HOLDING TORQUE IN PITCH AND ROLL DIRECTION AT EACH INTERNAL PRESSURE ON FEM SIMULATION

Internal pressure [MPa]	0.1	0.125	0.15	0.175	0.2
Magnification of holding torque	1.40	1.41	1.43	1.45	1.45

TABLE III
MAGNIFICATION OF HOLDING TORQUE IN PITCH AND ROLL DIRECTION AT EACH INTERNAL PRESSURE ON MEASUREMENT

Internal pressure [MPa]	0.1	0.125	0.15	0.175	0.2
Magnification of holding torque	1.80	1.53	1.45	1.57	1.65

TABLE IV
ERROR VALUES OF HOLDING TORQUE IN PITCH AND ROLL DIRECTIONS BETWEEN MEASURED AND FEM VALUES

Internal pressure [MPa]	0.1	0.125	0.15	0.175	0.2
Error in the pitch direction [%]	6.5	3.8	5.7	9.4	6.8
Error in the roll direction [%]	20.3	12.6	7.1	18.4	21.4

TABLE V
ERROR VALUES OF HOLDING TORQUE IN PITCH AND ROLL DIRECTIONS BETWEEN MEASURED AND THEORETICAL VALUES

Internal pressure [MPa]	0.1	0.125	0.15	0.175	0.2
Error in the pitch direction [%]	12.0	1.8	9.9	19.4	20.5
Error in the roll direction [%]	0.94	1.2	1.2	19.0	26.8

internal pressure. Tables II and III show the magnified FEM values between the pitch and roll directions and the magnification of the measurement values between the pitch and roll directions, respectively. Tables IV and V present the error values between the measured and FEM values as well as the measured and theoretical values, respectively.

In the theoretical model, the magnification between the holding torques in the pitch and roll directions is $\pi/2$ times, Table II indicates that the FEM values of the holding torque in the roll direction are on average 1.43 times larger than those in the pitch direction. Table III indicates that the measured values of the holding torque in the roll direction are on average 1.60 times larger than those in the pitch direction.

Table IV shows that the average errors between the measured and FEM values were approximately 6.5% and 16.0% in the pitch and roll directions, respectively. Table V shows that the average errors between the measured and theoretical values were approximately 12.7% and 9.8% in the pitch and roll

directions, respectively. Therefore, the results in Section IV show that the theoretical, measured, and FEM values are similar.

V. Discussion

The magnification of holding torques in the pitch and roll directions constructed in this letter can potentially be applied to other mechanisms with the 3-axis rotary joints. In the previously described wire method, which is one of the commonly adopted methods for variable stiffness mechanisms, there are 3-axis rotary bead joint shapes, and the relationship between the holding torque values in the pitch and roll directions is the same even in this method. It is possible to discuss the magnification of the joint holding torque in the pitch and roll directions in the absence of FEM with the wire method, because a highly nonlinear element of rubber tubes does not exist.

The rubber tube inside the structure may become twisted owing to the rotation of the ball joint in the rolling direction in the absence of pressure. Therefore, it is necessary to suppress rotation in the roll direction through geometrical constraints, for example, by placing a pin on the surface of the joint or covering it with a rubber membrane. However, it should be ensured that the maximum radius of curvature in the pitch direction is not decreased.

As the positive-pressurized mechanism in this study encloses a rubber tube, it has an extension effect in addition to the effect on the holding torque during pressurization. The soft actuator utilized the extension action generated by pressurizing each of the multiple chambers. Hence, it may be possible to change the characteristics of the mechanism by varying the material, shape, number, and arrangement of the chambers to be enclosed and adding the function of active extension in addition to variable stiffness.

Contrary to the tubes and airbags, the proposed mechanism does not form a linear shape when pressurized. When a non-stretchable tube is pressurized, it approaches a linear state corresponding to the maximum volume. In contrast, in the proposed mechanism, the internal volume of the rubber tube is constant regardless of the joint angle; thus, the fluid pressure does not generate torque around the joint angle. Although the fluid does not affect the rotation, the bending moment caused by the rubber tube material increases as the joint angle increases.

VI. Conclusion

This study presents a design method of variable stiffness mechanism with a 3-axis rotating ball joint that switches stiffness under positive pressure. Using a theoretical model of the torque required to hold the joint angle, we simulated the holding torque using the FEM and measured the holding torque in the pitch and roll directions when the actual pressure was applied. It was confirmed that the holding torque in the roll direction was $\pi/2$ times larger than that in the pitch direction for each value of internal pressure. This magnification can potentially be applied to other methods that use a 3-axis rotary joint. Furthermore, we also evaluated the FEM, theoretical and measured value of holding torque by numerical comparison.

In the future, we believe that this mechanism can be developed and applied in a wide range of fields. A potential application in the medical field is the use of guide endoscopes to design the structure of the proposed mechanism such that it is actively bendable (e.g., using the wire-driven method).

References

[1] M. Manti, V. Cacucciolo, and M. Cianchetti, "Stiffening in soft robotics: A review of the state of the art," *IEEE Robot. Automat. Mag.*, vol. 23, no. 3, pp. 93–106, Sep. 2016.

[2] L. Blanc, A. Delchambre, and P. Lambert, "Flexible medical devices: Review of controllable stiffness solutions," *Actuators*, vol. 6, no. 3, pp. 1–31, 2017.

[3] E. Brown et al., "Universal robotic gripper based on the jamming of granular material," *Proc. Nat. Acad. Sci.*, vol. 107, no. 44, pp. 18809–18814, 2010.

[4] Y. Wei, Y. Chen, Y. Yang, and Y. Li, "A soft robotic spine with tunable stiffness based on integrated ball joint and particle jamming," *Mechatronics*, vol. 33, pp. 84–92, 2016.

[5] M. Fujita et al., "Jamming layered membrane gripper mechanism for grasping differently shaped-objects without excessive pushing force for search and rescue missions," *Adv. Robot.*, vol. 32, no. 11, pp. 590–604, 2018.

[6] Y. J. Kim, S. Cheng, S. Kim, and K. Iagnemma, "A novel layer jamming mechanism with tunable stiffness capability for minimally invasive surgery," *IEEE Trans. Robot.*, vol. 29, no. 4, pp. 1031–1042, Aug. 2013.

[7] D. C. F. Li, Z. Wang, B. Ouyang, and Y. H. Liu, "A reconfigurable variable stiffness manipulator by a sliding layer mechanism," in *Proc. Int. Conf. Robot. Autom.*, 2019, pp. 3976–3982.

[8] M. Ibrahimi, L. Paternò, L. Ricotti, and A. Menciassi, "A layer jamming actuator for tunable stiffness and shape-changing devices," *Soft Robot.*, vol. 8, no. 1, pp. 85–96, 2021.

[9] A. Degani, H. Choset, B. Zubiate, T. Ota, and M. Zenati, "Highly articulated robotic probe for minimally invasive surgery," in *Proc IEEE Int. Conf. Robot. Autom.*, 2006, pp. 4167–4172.

[10] Y. J. Kim, S. Cheng, S. Kim, and K. Iagnemma, "A stiffness-adjustable hyper-redundant manipulator using a variable neutral-line mechanism for minimally invasive surgery," *IEEE Trans. Robot.*, vol. 30, no. 2, pp. 382–395, Apr. 2014.

[11] Y. Jiang, D. Chen, C. Liu, and J. Li, "Chain-Like granular jamming: A novel stiffness-programmable mechanism for soft robotics," *Soft Robot.*, vol. 6, no. 1, pp. 118–132, 2019.

[12] R. Mukaide et al., "Radial-layer jamming mechanism for string configuration," *IEEE Robot. Automat. Lett.*, vol. 5, no. 4, pp. 5221–5228, Oct. 2020.

[13] H. Nakai, Y. Hoshino, M. Inaba, and H. Inoue, "Softening deformable robot: Development of shape adaptive robot using phase change of low-melting-point alloy," *J. Robot. Soc. Jpn.*, vol. 20, no. 6, pp. 625–630, 2002.

[14] B. E. Schubert and D. Floreano, "Variable stiffness material based on rigid low-melting-point-alloy microstructures embedded in soft poly (dimethylsiloxane) (PDMS)," *RSC Adv.*, vol. 3, no. 46, pp. 24671–24679, 2013.

[15] W. Shan, T. Lu, and C. Majidi, "Soft-matter composites with electrically tunable elastic rigidity," *Smart Mater. Structures*, vol. 22, no. 8, 2013, Art. no. 05201.

[16] A. J. Loeve, J. H. Bosma, P. Breedveld, D. Dodou, and J. Dankelman, "Polymer rigidity control for endoscopic shaft-guide 'plastolock' - A feasibility study," *J. Med. Devices*, vol. 4, no. 4, pp. 1–6, 2010.

[17] W. Shan, S. Diller, A. Tutcuoglu, and C. Majidi, "Rigidity-tuning conductive elastomer," *Smart Mater. Structures*, vol. 24, no. 6, 2015, Art. no. 065001.

[18] A. Balasubramanian, M. Standish, and C. J. Bettinger, "Microfluidic thermally activated materials for rapid control of macroscopic compliance," *Adv. Funct. Mater.*, vol. 24, no. 30, pp. 4860–4866, 2014.

[19] M. Mizutani, Y. Shimodate, and K. Ito, "Semicircular duplex manipulator to search narrow spaces for victims," in *Proc. IEEE Int. Conf. Saf., Secur., Rescue Robot.*, 2011, pp. 7–12.

[20] T. Miller-Jackson, Y. Sun, R. Natividad, and C. H. Yeow, "Tubular jamming: A variable stiffening method toward high-force applications with soft robotic components," *Soft Robot.*, vol. 6, no. 4, pp. 468–482, 2019.

[21] C. Sozer, L. Paternò, G. Tortora, and A. Menciassi, "A novel pressure-controlled revolute joint with variable stiffness," *Soft Robot.*, vol. 9, no. 4, pp. 723–733, 2021.

[22] Y. Nakata, "Tool holding articulated arm," U.S. Patent 20160151920, Jun. 2, 2016.

[23] I. Onda, M. Watanabe, K. Tadakuma, E. Takane, M. Konyo, and S. Tadokoro, "Pneumatic driven hollow variable stiffness mechanism aiming non-contact insertion of telescopic guide tubes," in *Proc. IEEE 4th Int. Conf. Soft Robot.*, 2021, pp. 615–621.

[24] I. Onda et al., "Highly articulated tube mechanism with variable stiffness and shape restoration using a pneumatic actuator," *IEEE Robot. Automat. Lett.*, vol. 7, no. 2, pp. 3664–3671, Apr. 2022.